JOURNAL OF APPLIED ELECTROCHEMISTRY 25 (1995) 1017–1022

A wall-jet electrode reactor and its application to the study of electrode reaction mechanisms Part I: Design and construction

P. LAEVERS, A. HUBIN, H. TERRYN, J. VEREECKEN

Department of Metallurgy, Electrochemistry and Materials Science, Vrije Universiteit Brussel, Pleinlaan 2, 1050 Brussels, Belgium

Received 30 January 1995; revised 24 April 1995

A wall-jet electrode reactor possessing a laminar flow regime, suitable for mechanistic studies, is reported. This reactor is different from those described in the literature in the size of its working electrode surface area. The reactor is evaluated by means of mass transport–limited current measurements using as a model reaction the reduction of ferricyanide ions at a platinum electrode surface from a 0.01 M $K_3Fe(CN)_6$–0.01 M $K_4Fe(CN)_6$ solution containing 1 M KCl as supporting electrolyte. The dependence of the mass transport–limited current on the crucial reactor parameters – the volume flow rate V_f ($m^3 s^{-1}$), the nozzle diameter a (m) and the radius of the working electrode R (m) – is established and verified by theoretical predictions. The reactor is shown to have the desired wall-jet hydrodynamics for: $1.6 \times 10^{-6} \leqslant V_f \leqslant 4.3 \times 10^{-6} m^3 s^{-1}$, $1.5 \times 10^{-3} \leqslant a \leqslant 3 \times 10^{-3} m$ and $1.5 \times 10^{-2} \leqslant R \leqslant 2 \times 10^{-2} m$.

List of symbols

a	nozzle diameter (m)
C_A	concentration of A in the bulk ($mol\,m^{-3}$)
D_A	diffusion coefficient of A ($m^2 s^{-1}$)
F	Faraday's constant ($C\,mol^{-1}$)
η	dynamic viscosity ($g\,m^{-1} s^{-1}$)
H	distance between the working electrode and the tip of the nozzle (m)
I_{lim}	mass-transport-limited current (A)
k_r	constant linking the typical velocity of the wall-jet to the mean velocity in the nozzle
ν	kinematic viscosity ($m^2 s^{-1}$)
n	number of electrons exchanged
ρ	density ($g\,m^{-3}$)
R	radius of the working electrode (m)
t	time (s)
V_f	volume flow rate ($m^{-3} s^{-1}$)

1. Introduction

Our research on the mechanism of the a.c. electrolytic graining of rolled aluminium substrates [1–6] has developed to the stage where the designated means to achieve further insight into this controlled corrosion process is a quantitative electrochemical investigation of the mechanism of the electrode reactions involved.

A quantitative electrochemical study of electrode reaction mechanisms typically includes voltammetric and step experiments in a well defined hydrodynamic electrode system, to examine the influence of mass transport on the current–potential and transient characteristics and comparison of the experimentally determined diagrams with calculated ones derived from candidate mechanistic schemes.

It has been established that the wall-jet electrode system possessing a laminar flow regime (for the sake of simplicity, termed 'the wall-jet electrode system' throughout this and the subsequent papers of this series) has a high mechanistic resolution compared to other hydrodynamic electrode systems (e.g., rotating disc or channel electrode), due to the highly nonuniform accessibility of the electrode surface [7]. The theoretical evaluation of the use of the wall-jet electrode system in a quantitative electrochemical study has been developed by Compton *et al.* [8–15]. In the wall-jet electrode system the flow is due to a submerged fluid jet impinging perpendicularly onto a planar electrode and spreading out radially over the electrode surface, the fluid outside the jet being at rest [16]. The pattern of flow is schematically illustrated in Fig. 1. It can be subdivided into four hydrodynamic characteristic regions: the potential core, the free-jet region, the stagnation zone and the wall-jet region [17–22]. As the flow discharges from the submerged nozzle, the fluid in the jet exchanges momentum with the surrounding fluid, creating a free-jet. This leaves a conical potential core in which the pipe flow properties at the nozzle exit are retained. The core length varies from 4 to 8 nozzle diameters depending on the shape of the nozzle. By the intensive exchange of momentum over the free boundaries, the jet broadens linearly along its downstream direction up to a limiting distance, 1.2 to 2.2 nozzle diameters from the electrode surface, that marks the boundary of the stagnation flow region. In the stagnation zone the flow is deflected by the surface; its axial velocity

0021-891X

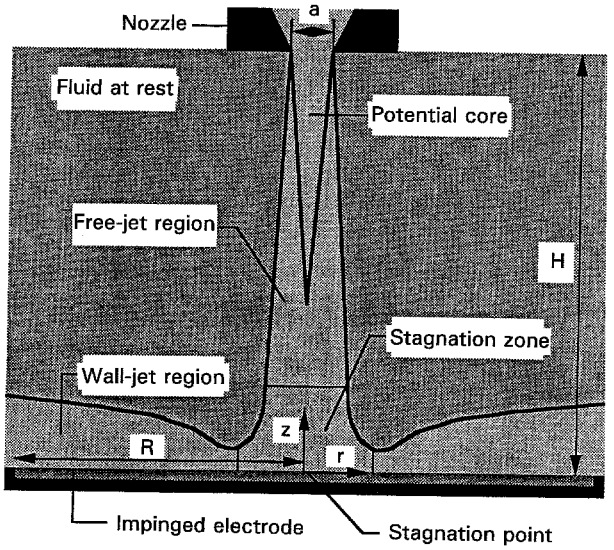

Fig. 1. The pattern of flow in a wall-jet electrode system.

is decelerated and transformed into an accelerating one parallel to the electrode surface. Due to the exchange of momentum with the quiescent surrounding fluid, the accelerating stagnation flow must transform into a decelerating wall-jet. The velocity parallel to the electrode surface reaches its maximum 0.6 to 1.4 nozzle diameters from the stagnation point, where the stagnation zone passes into the wall-jet region. In the wall-jet region the flow is influenced by the electrode surface as well as by the quiescent surrounding fluid. From this pattern of flow it is clear that the wall-jet electrode system has a highly nonuniformly accessible electrode surface; the rates of mass transport are much higher in the centre of the electrode than at the edge.

To use the wall-jet electrode system in the quantitative electrochemical study of the mechanism of the a.c. electrolytic graining of rolled aluminium substrates, a suitable wall-jet electrode reactor had to be designed, since the a.c. electrolytic graining of rolled aluminium is strongly influenced by the substrate conditions [6] and a study of the mechanism of the electrode processes involved thus requires representative samples of the rolled substrate, i.e. samples with a large surface area. The reactor developed is therefore different from others designed for mechanistic purposes [15, 23–25] in the size of its working electrode surface area and different from other wall-jet electrode reactors possessing large target electrodes [18–20] in its laminar flow regime.

In this paper the design and construction of the wall-jet electrode reactor is reported and evaluated. In a second paper, a numerical computational method is put forward to solve the mass transport problems involved in using the wall-jet electrode reactor as a hydrodynamic electrode system in a quantitative electrochemical investigation of electrode reaction mechanisms. The numerical scheme developed, is designed to allow the computations to be performed on a personal computer. In a third paper the quantitative electrochemical investigation of the mechanism of the electrode processes involved in the a.c. electrolytic graining of rolled aluminium substrates will be reported.

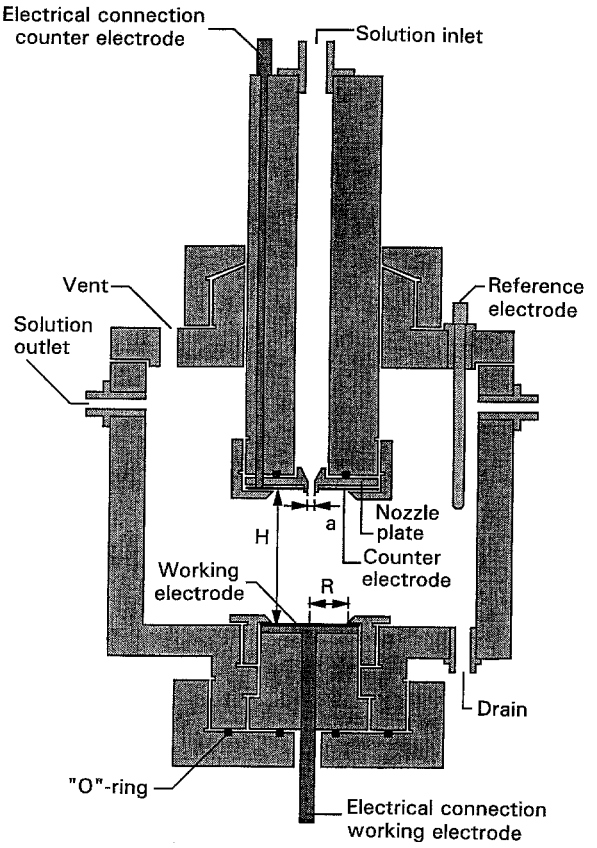

Fig. 2. The wall-jet electrode reactor.

2. Design and setup of the wall-jet electrode reactor

The necessity of a large impinged electrode restrains the ranges of all other reactor parameters for which true wall-jet hydrodynamics under a laminar flow regime are to be expected [22, 23]. The reactor was designed accordingly.

The design and construction details of the wall-jet electrode reactor are shown in Fig. 2. The complete setup is schematically outlined in Fig. 3. Its main components, besides the reactor, are: a thermostatically controlled reservoir, a membrane pump and a set of rotameters. The reactor is entirely machined from a PVC rod. The main body, 2.00×10^{-1} m in diameter and 1.50×10^{-1} m in height, is sealed off by a cover plate in which five holes of diameter 1.00×10^{-2} m prevent evolving gases from accumulating. The body and cover plate are secured to one another by six bolts. The slide-fitting extension at the centre of the cover plate accommodates a tube, 2.00×10^{-2} m in inner diameter, carrying the nozzle plate and counter electrode. The screw cap on top of the extension, when tightened, pinches off the slide-fitting, allowing the distance between the tip of the nozzle and the working electrode to be set. This distance can range between 5.0×10^{-3} and 1.200×10^{-1} m. The counter electrode, a thin disc ($\pm 6.5 \times 10^{-2}$ m in diameter) of the desired material, is mounted concentrically and level with the tip of the nozzle. The electrical connection is made by

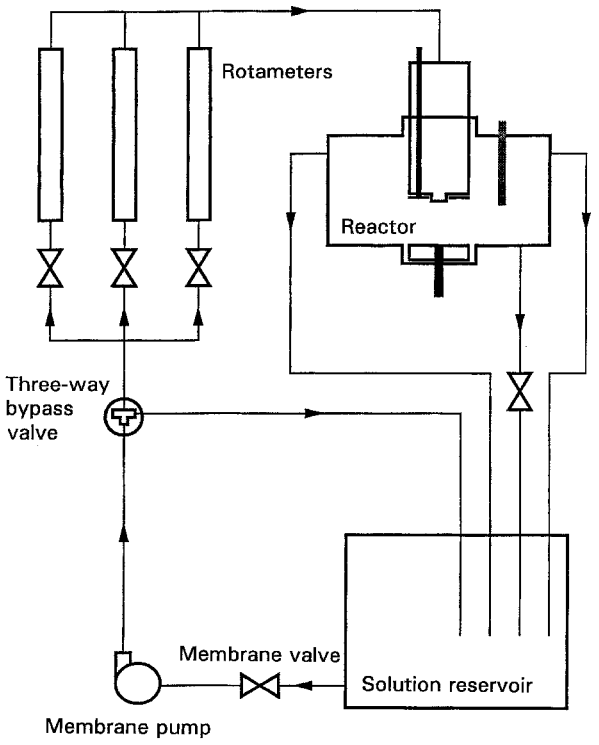

Fig. 3. Setup of the wall-jet electrode reactor.

the aluminium rod, press-fitted in the wall of the carrying tube. The nozzle plate and counter electrode are secured to the tube by a screw cap, leaving an active surface area of $1.256 \times 10^{-3}\,m^2$. The Viton™ O-ring seals this section. Four nozzle plates having a diameter of 1.50, 2.00, 2.50 and 3.00×10^{-3} m are available. A suitable hole in the cover plate accommodates the saturated calomel reference electrode. It is mounted so as not to disturb the flow pattern of the impinging jet. At the bottom centre of the main body a screw-in extension is machined to accommodate the working electrode. The working electrode, a thin disc ($\pm 5.5 \times 10^{-2}$ m in diameter) of the desired material, is clasped between the electrode holder and the T-shaped aluminium rod, press-fitted in an insulating holder, ensuring electrical connection. This whole section is sealed by the screw cap which, when tightened, compresses the set of Viton™ O-rings. The active surface of the working electrode is determined by the electrode holder. Five holders with an opening of radius 1.500, 1.625, 1.750, 1.875 and 2.000×10^{-2} m are available. The solution is passed through the system by an entirely Teflon coated membrane pump (KNF ND.1300 TTE, Verder). The feed rate of solution to the reactor is controlled by a three-way bypass valve and a set of membrane valves upstream of the pump and the rotameters. The valves are made of PVC; the membranes and fittings are made of Viton™ . A set of glass tube rotameters with titanium floats (Rota Yokogawa) are used to measure the feed rate. The solution reservoir is a 42 litre high-density polyethylene tank provided with a glass heat exchanger connected to a circulation thermostat (FE2, Haake) with flexible PVC tubing. Connections between all components are made by PVC tube and fittings, 1.20×10^{-2} m in inner diameter.

3. Experimental details

The mass transport–limited current measurements (i.e., the current transient measurements) were carried out for the reduction of ferricyanide ions, at a platinum electrode surface, from a 0.01 M $K_3Fe(CN)_6$–0.01 M $K_4Fe(CN)_6$ solution containing 1 M KCl as supporting electrolyte. The solution was prepared from analytical grade reagents and deionized water. Its dynamic viscosity, $\eta = 0.89\,g\,m^{-1}\,s^{-1}$, and density, $\rho = 1.05 \times 10^6\,g\,m^{-3}$, were measured by means of a Haake microviscosimeter and a gravimetric experiment respectively. The working electrode was polished to a mirror finish on a DIP 10 Struers polishing table using successively finer diamond lapping compounds, down to 1 μm. Between experiments the working electrode was polished by hand with 1 μm diamond paste, to ensure the reproducibility of experiments. The counter electrode used, was a platinum disk 5.0×10^{-4} m thick and 6.50×10^{-2} m in diameter, with a concentric hole 5.0×10^{-3} m in diameter. A Solartron Electrochemical Interface 1186, combined with an Amel 567 function generator, was used to step the potential of the working electrode from its equilibrium potential ($E_0 = 2.28 \times 10^{-1}$ V vs SCE) to a potential for which mass transport is controlling the rate of reaction (between -4.50×10^{-1} and -5.00×10^{-1} V vs SCE, depending on the reactor parameters used). The latter was determined by voltammetric experiments, where the potential of the working electrode was linearly swept from $+2.50 \times 10^{-1}$ to -7.00×10^{-1} V with respect to a saturated calomel reference electrode, using a scan rate of $3 \times 10^{-3}\,V\,s^{-1}$. The linear sweep voltammograms and current transients were recorded on a Nicolet 310 oscilloscope. All experiments were carried out under thermostatic conditions at 25 ± 0.5 °C.

4. Results and discussion

For a simple electron transfer reaction

$$A \pm ne^- \rightarrow B$$

an analytical expression has been derived [23, 24, 26, 27] establishing the dependence of the mass transport-limited current on the crucial parameters of the wall-jet electrode system

$$I_{lim} = \pm 1.59\, k_r n F D_A^{2/3} \nu^{-5/12} V_f^{3/4} a^{-1/2} R^{3/4} C_A^{bulk} \quad (1)$$

where n is the number of electrons exchanged, F ($C\,mol^{-1}$) is the faradaic constant, D_A ($m^2\,s^{-1}$) is the diffusion coefficient of A, ν ($m^2\,s^{-1}$) is the kinematic viscosity of the electrolyte solution, V_f ($m^3\,s^{-1}$) is the volume flow rate, a (m) is the nozzle diameter, R (m) is the radius of the working electrode, C_A^{bulk} ($mol\,m^{-3}$) is the concentration of A in the bulk and k_r is a constant linking the typical velocity of the wall-jet to the mean velocity in the nozzle. The

reactor constant k_r has to be determined by experiment.

The wall-jet electrode reactor is therefore evaluated by means of mass transport–limited current measurements using as a model reaction the reduction of ferricyanide ions at a platinum electrode surface; the dependence of the mass transport–limited current on the crucial reactor parameters is established.

The mass transport–limited current values reported below are the arithmetic mean of ten measured values, the variance between them being less than 1×10^{-3} A. Typical examples of the transients, from which the mass transport–limited current is derived, are shown in Fig. 4. As can be seen, the chronoamperometric transients recorded are well defined, exhibiting fluctuations of the steady state mass transport–limited current which do not exceed 1% of the corresponding geometrical average, which is used as the measured value of the mass transport–limited current.

4.1. *Influence of the distance between the working electrode and the tip of the nozzle*

Although the theoretical mass transport–limited current equation does not contain the distance H (m) between the working electrode and the tip of the nozzle as a parameter, it can easily be understood from the pattern of flow shown in Fig. 1, that this parameter, or more particularly, its ratio to the nozzle diameter – as the dimension of the characteristic regions in the pattern of flow are closely related to the nozzle diameter – determines whether or not true wall-jet electrode hydrodynamics can be achieved in the reactor. If the ratio of H to the nozzle diameter is too small, a nondeveloped free-jet impinges on the surface of the working electrode, deviating the fluid dynamics from the desired wall-jet electrode hydrodynamics. On the other hand, if the ratio is too large, the free-jet spreads out before it hits the surface of the working electrode and again the hydrodynamics deviate from the desired conditions. Therefore the range of H/a in which the mass transport–limited current is unaffected by the nozzle tip to working electrode separation was established for the various nozzle plates available and found to be $12 \leqslant H/a \leqslant 15$. For all experiments reported below, the ratio of H to the nozzle diameter was set in accordance with this finding.

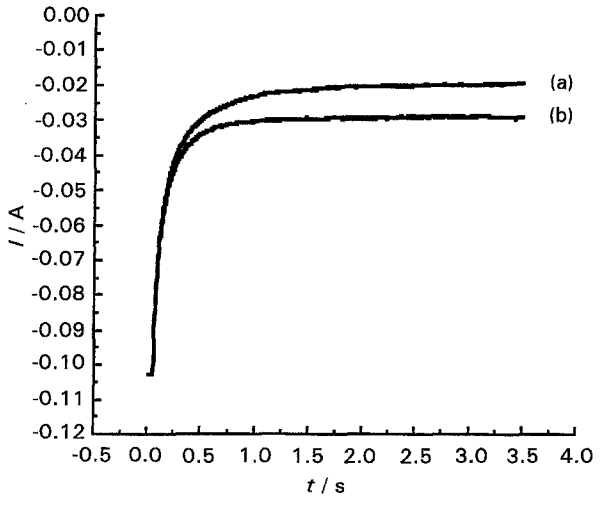

Fig. 4. Typical examples of the chronoamperometric transients recorded in the wall-jet electrode reactor presented, for the reduction of ferricyanide ions at a platinum electrode surface from a 0.01 M $K_3Fe(CN)_6$–0.01 M $K_4Fe(CN)_6$ solution containing 1 M KCl as supporting electrolyte ($E_0 = 2.28 \times 10^{-1}$ V vs SCE, $E = -4.50 \times 10^{-1}$ V vs SCE for (a) and -4.70×10^{-1} V vs SCE for (b), $R = 2.000 \times 10^{-2}$ m, $a = 2.00 \times 10^{-3}$ m, $H/a = 13$). (a) $V_f = 1.689 \times 10^{-6}$ m^3 s^{-1}; (b) $V_f = 2.981 \times 10^{-6}$ m^3 s^{-1}.

4.2. *Dependence on the volume flow rate*

The theoretically derived mass transport–limited current equation indicates, that I_{lim} is proportional to the 3/4ths power of the volume flow rate. This proportionality was verified in the wall-jet electrode reactor presented, for a wide range of volume flow rates and three settings of the radius of the working electrode relative to the nozzle diameter ((a) $R = 1.750 \times 10^{-2}$ m, $a = 2.00 \times 10^{-3}$ m; (b) $R = 2.000 \times 10^{-2}$ m, $a = 2.00 \times 10^{-3}$ m; (c) $R = 2.000 \times 10^{-2}$ m, $a = 1.50 \times 10^{-3}$ m). The log–log plots of the mass transport–limited current as a function of the volume flow rate, shown in Fig. 5, are good straight lines with slopes ranging from 0.71 to 0.74. This is in good agreement with the theoretical value.

4.3. *Dependence on the nozzle diameter*

In accordance with the theoretical mass transport–limited current equation, I_{lim} is expected to be inversely proportional to the 1/2th power of the nozzle diameter in the reactor being evaluated. To examine this proportionality, the mass transport–limited current was measured for the various nozzle plates available ($a = 1.50$, 2.00, 2.50 and 3.00×10^{-3} m), under two conditions of the volume flow rate relative to the radius of the working

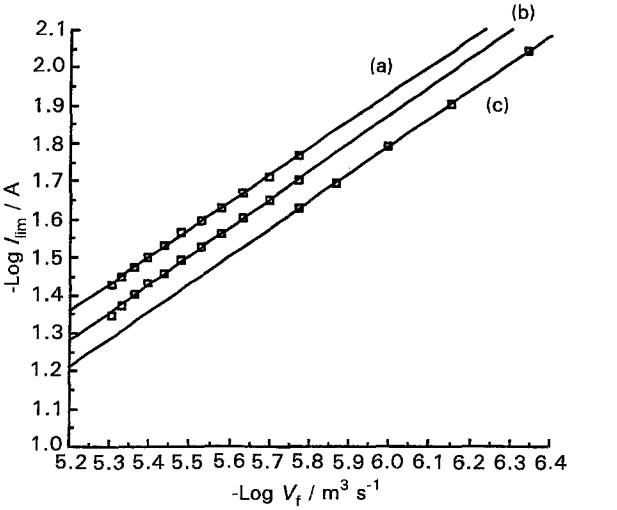

Fig. 5. Dependence of the mass transport–limited current on the volume flow rate in the wall-jet electrode reactor presented. (a) $R = 1.750 \times 10^{-2}$ m, $a = 2.00 \times 10^{-3}$ m; (b) $R = 2.000 \times 10^{-2}$ m, $a = 2.00 \times 10^{-3}$ m; (c) $R = 2.000 \times 10^{-2}$ m, $a = 1.50 \times 10^{-3}$ m; $H/a = 13$

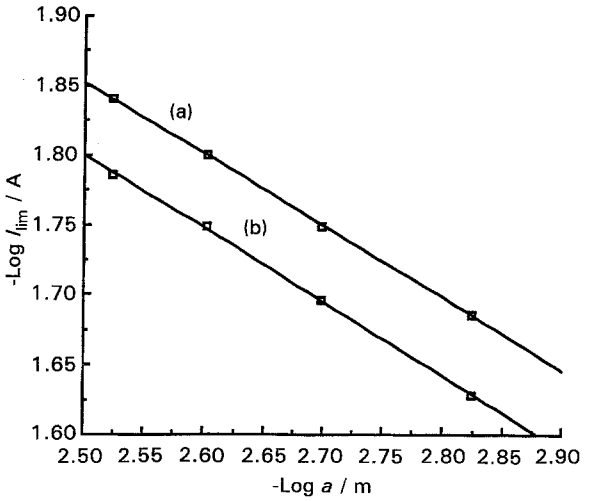

Fig. 6. Dependence of the mass transport–limited current on the nozzle diameter in the wall-jet electrode reactor presented. (a) $V_f = 1.689 \times 10^{-6}\,m^3\,s^{-1}$, $R = 1.750 \times 10^{-2}\,m$; (b) $V_f = 2.981 \times 10^{-6}\,m^3\,s^{-1}$, $R = 2.000 \times 10^{-2}\,m$; $H/a = 13$.

electrode ((a) $V_f = 1.689 \times 10^{-6}\,m^3\,s^{-1}$, $R = 1.750 \times 10^{-2}\,m$; (b) $V_f = 2.981 \times 10^{-6}\,m^3\,s^{-1}$, $R = 2.000 \times 10^{-2}\,m$). The results obtained are shown in Fig. 6. This log–log diagram of the mass transport–limited current versus the nozzle diameter shows two good straight lines with a slope of −0.52 and −0.53, being in good agreement with the theoretical value.

4.4. *Dependence on the radius of the working electrode*

The theoretical mass transport–limited current depends on the 3/4th power of the radius of the working electrode. Figure 7 shows a logarithmical plot establishing the dependence of I_{lim} on the radius of the working electrode in the wall-jet electrode reactor being evaluated. The dependence was examined over a range of R from 1.500 to $2.000 \times 10^{-2}\,m$, for three settings of the volume flow rate relative to the nozzle diameter ((a) $V_f = 1.689 \times 10^{-6}\,m^3\,s^{-1}$, $a = 2.00 \times 10^{-3}\,m$; (b) $V_f = 1.689 \times 10^{-6}\,m^3\,s^{-1}$, $a = 1.50 \times 10^{-2}\,m$; (c) $V_f = 2.981 \times 10^{-6}\,m^3\,s^{-1}$, $a = 2.00 \times 10^{-2}\,m$). The plots shown are good straight lines with slopes ranging from 0.75 to 0.78. These values compare well with the theoretical.

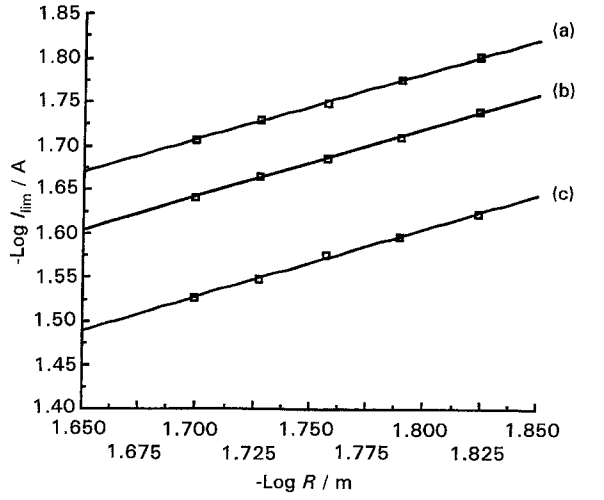

Fig. 7. Dependence of the mass transport–limited current on the radius of the working electrode in the wall-jet electrode reactor presented. (a) $V_f = 1.689 \times 10^{-6}\,m^3\,s^{-1}$, $a = 2.00 \times 10^{-3}\,m$; (b) $V_f = 1.689 \times 10^{-6}\,m^3\,s^{-1}$, $a = 1.50 \times 10^{-2}\,m$; (c) $V_f = 2.981 \times 10^{-6}\,m^3\,s^{-1}$, $a = 2.00 \times 10^{-2}\,m$, $H/a = 13$.

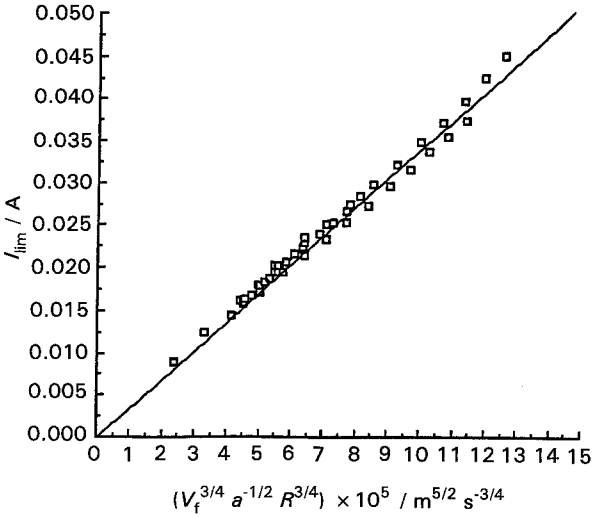

Fig. 8. Determination of the reactor constant for the wall-jet electrode reactor presented.

4.5. *Determination of the reactor constant*

In order to determine k_r for the wall-jet electrode reactor, all data obtained establishing its dependence on the volume flow rate, the nozzle diameter and the radius of the working electrode, are brought together in one diagram plotting the mass transport–limited current as a function of $(V_f^{3/4} a^{-1/2} R^{3/4})$, as shown in Fig. 8. From the slope of the straight line fitted through the experimental values, the reactor constant was calculated to be 0.82 using $7.7 \times 10^{-10}\,m^2\,s^{-1}$ for the diffusion coefficient of ferricyanide ions [28] and $0.85 \times 10^{-6}\,m^2\,s^{-1}$ for the kinematic viscosity of the solution. As k_r is the proportionality factor between the typical velocity of the wall-jet and the mean velocity in the nozzle, a value of the order of unity is reasonable.

5. Conclusions

The reactor presented has the desired wall-jet electrode hydrodynamics for $1.6 \times 10^{-6} \leqslant V_f \leqslant 4.3 \times 10^{-6}\,m^3\,s^{-1}$, $1.5 \times 10^{-3} \leqslant a \leqslant 3 \times 10^{-3}\,m$ and $1.5 \times 10^{-2} \leqslant R \leqslant 2 \times 10^{-2}\,m$, making it a powerful tool in the mechanistic study of electrode processes, especially for processes requiring a large electrode surface area, such as the a.c. electrolytic graining of rolled aluminium substrates.

Quantitative information on the mechanism of electrode processes can be obtained by fitting calculated to experimentally determined voltammograms, current or voltage transients. In order to do so, a computational method is required, solving the mass transport problems involved in using the wall-jet electrode reactor.

Acknowledgements

The authors thank M. De Pauw and M. Raes for the technical realization of the reactor and the experimental work performed, respectively. The financial support of P. Laevers by I.W.T. (Vlaams Instituut voor de Bevordering Van het Wetenschappelijk-Technologisch Onderzoek in de Industrie) is gratefully acknowledged.

References

[1] H. Terryn, J. Vereecken and G. E. Thompson, *Trans. Inst. Metal Finishing* **66** (1988) 116.
[2] *Idem, Corros. Sci.* **32** (1991) 1159.
[3] *Idem, ibid.* **32** (1991) 1173.
[4] P. Laevers, H. Terryn and J. Vereecken, *Trans. Inst. Metal Finishing* **70**(3) (1992) 105.
[5] P. Laevers, H. Terryn, J. Vereecken and G. E. Thompson, *Corros. Sci.* **35** (1993) 231.
[6] P. Laevers, H. Terryn, J. Vereecken, B. Kernig and B. Grzemba, accepted for publication in *Corros. Sci.*
[7] R. G. Compton, A. C. Fisher and G. P. Tyley, *J. Appl. Electrochem.* **21** (1991) 295.
[8] R. G. Compton, C. R. Greaves and A. M. Waller, *ibid.* **20** (1990) 575.
[9] *Idem, ibid.* **20** (1990) 586.
[10] R. G. Compton, A. C. Fisher and G. P. Tyley, *ibid.* **20** (1990) 912.
[11] *Idem, ibid.* **21** (1991) 2.
[12] A. C. Fisher, R. G. Compton, C. M. A. Brett and A. M. C. F. Oliveira Brett, *J. Electroanal. Chem.* **318** (1991) 53.
[13] R. G. Compton, A. C. Fisher, M. H. Latham, C. M. A. Brett and A. M. C. F. Oliveira Brett, *J. Appl. Electrochem.* **22** (1992) 1011.
[14] *Idem, J. Phys. Chem.* **96**(21) (1992) 8363.
[15] C. M. A. Brett, A. M. C. F. Oliveira Brett, A. C. Fisher and R. G. Compton, *J. Electroanal. Chem.* **334** (1992) 57.
[16] M. B. Glauert, *J. Fluid Mech.* **1** (1956) 625.
[17] H. Marin, 'Advances in heat transfer', vol. 13 (edited by J. P. Hartnett and T. F. Irvine Jr.), Academic Press, New York (1977).
[18] E. A. Vallis, M. A. Patrick and A. A. Wragg, Proceedings of AIChE Meeting, New York (1977).
[19] *Idem*, Proc. Euromech., Nancy (1977).
[20] *Idem*, Proceedings of the International Heat Transfer Conference, Toronto, vol. 5 (1978) p. 297.
[21] D. T. Chin and C. H. Tsang, *J. Electrochem. Soc.* **125**(3) (1978) 1461.
[22] F. P. Incropera and D. P. De Witt, 'Fundamentals of heat and mass transfer', John Wiley & Sons, New York (1990).
[23] J. Yamada and H. Matsuda, *J. Electroanal. Chem.* **44** (1973) 189.
[24] W. J. Albery and C. M. A. Brett, *ibid.* **148** (1983) 211.
[25] R. G. Compton, C. R. Greaves and A. M. Waller, *J. Appl. Electrochem.* **20** (1990) 586.
[26] H. Matsuda, *J. Electroanal. Chem.* **16** (1968) 153.
[27] W. J. Albery and C. M. A. Brett, *ibid.* **148** (1983) 201.
[28] S. Vandeputte, B. Tribollet, A. Hubin and J. Vereecken, *Electrochim. Acta* **33**(18) (1994) 2729.